



Implementing Crowbar Protection To Maintain System Stability In Doubly Fed Induction Generator Wind Turbines

Nassira Medjadji ^{a,*}, Driss Meddah Medjahed ^a, Abdelkader Mahamedi ^b, Kaddour Abdelmajid ^c, Mostapha Yahiaoui ^a, Abdelkader Aris ^d

^a Artificial Intelligence Laboratory for Mechanical and Civil Structures, and Soil, University Center of Naama, P.O. Box 66, Naama 45000, Algeria

^b Ziane Achour University, Djelfa 17000, Algeria

^c Unité de Recherche Appliquée en Energies Renouvelables, URAER, Centre de Développement des Energies Renouvelables, CDER, 47133, Ghardaïa, Algeria

^d Department of Mechanical Engineering ENPO, 31000, Algeria

ARTICLE INFO

Article history:

Received September 19, 2024

Accepted October 21, 2024

Keywords:

Wind energy,
Doubly field induction
Regulation,
DFIG.

ABSTRACT

Doubly fed induction generator (DFIG) wind turbines play a crucial role in wind energy production. However, system stability during symmetrical voltage dips remains a significant challenge. This research area focuses on enhancing protection and regulation strategies to ensure that DFIG wind turbines operate stably and efficiently even when the electrical grid experiences disturbances. In-depth simulations and behavioral analyses are utilized to propose effective control solutions, minimizing the impact of voltage dips without compromising system stability. The findings from these studies are essential for wind turbine manufacturers and operators, contributing to the overall improvement of wind energy systems.

1. INTRODUCTION

In the context of renewable energy production, wind farms are increasingly prominent (Hughes, 2005; Rabelo et al., 2008). Among various types of wind turbines, those equipped with a doubly fed induction generator (DFIG) are widely utilized due to their advantages in energy efficiency and power control (Canudas de Wit, 2000; Seyoum et al., 2003). However, these systems are susceptible to disturbances such as symmetrical voltage dips, which can impact their stability and performance (Abad et al., 2011).

Symmetrical voltage dips manifest as abrupt, momentary drops in electrical grid voltage. They arise from various sources like short circuits, network faults, or concurrent electrical equipment operation

* Corresponding author, E-mail address: medjadji@univ-naama.dz

Tel : + 213 793152487



(Csanyi, 2013). Such disturbances induce transient fluctuations in both electrical and mechanical parameters of the DFIG, potentially compromising its stability and capacity for consistent grid power supply (Idjdarene et al., 2008; Karad & Thakur, 2021).

In this study, our primary objective is to refine protective measures and regulatory methods aimed at upholding the stability of DFIG systems amidst symmetrical voltage dips. Our investigation delves into various busbar protection methodologies, including the implementation of busbar resistances, designed to sustain wind turbine connectivity to the grid amid episodes of symmetrical voltage dips. Additionally, we scrutinize regulatory tactics geared towards mitigating transient impacts on rotor speed, thereby ensuring the consistent and stable operation of the system (Tamvada & Babu, 2022).

2. DESCRIPTION OF A DFIG-BASED WIND ENERGY CONVERSION SYSTEM

We start by outlining the different elements of a wind turbine utilizing the Doubly Fed Induction Generator (DFIG), a popular choice for wind energy generation owing to its adaptability and superior efficiency, as depicted in Figure 1. The system comprises these parts:

2.1 Wind power

The source relied upon for providing energy in this system is the wind.

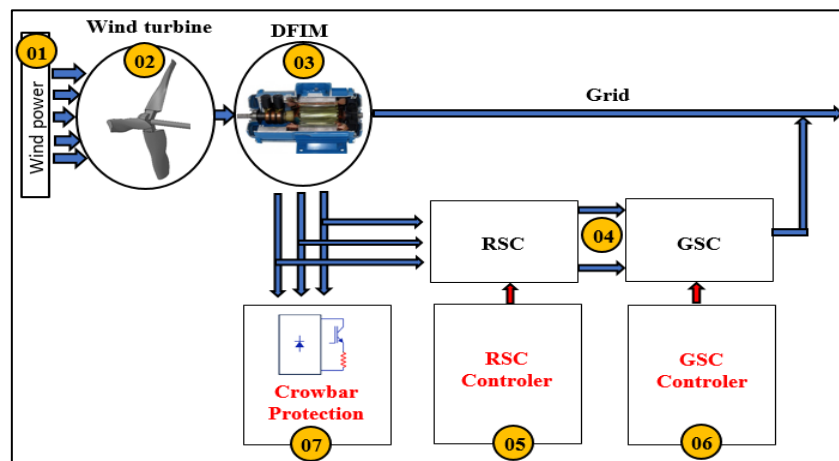


Fig 1. General Structure of Different Parts of the System

2.2 Wind Turbine Modeling

A wind turbine is an apparatus designed to transform the motion energy of the wind into either mechanical or electrical energy. Typically, it comprises a rotor featuring blades, a generator, and supportive frameworks like a tower (refer to Fig. 1).

2.2.1 Mechanical Power of the Wind Turbine

The kinetic power calculated with:

$$P_{incident} = \frac{1}{2} \cdot \rho \cdot S \cdot V^3 \quad (1)$$

Where:

ρ : Air density [kg/m³]

S : Area swept by the rotor [m²],

V : Wind speed [m/s].

The aerodynamic power of the wind turbine [W] is:

$$P_{aero} = \frac{1}{2} \cdot \rho \cdot \pi \cdot R^2 \cdot C_p(\lambda, \beta) \cdot V_{wind}^3 \quad (2)$$

V_{wind} : Wind speed [m/s]

R : Radius of the wind turbine [m]

ρ : Air density [kg/m³]

C_p : Power coefficient

λ : Relative velocity [m/s]

β : Blade pitch angle in degrees (°)

2.2.2 Power Coefficient

The aerodynamic efficiency is represented by the power coefficient C_p :

$$\begin{cases} C_p = (c_1 - c_2)(\beta - c_3) \sin(A) - c_4(\lambda - c_5)(\beta - c_3) \\ A = \frac{\pi(\lambda+0.1)}{18.5-0.3(\beta-2)} \end{cases} \quad (3)$$

Where the coefficient values c_1 – c_5 chosen are :

$$C_1=0.5, C_2=0.167, C_3=2, C_4=0.00184, C_5=3$$

2.1.3 Relative Velocity

We introduce a variable called relative velocity:

$$\lambda = \frac{\Omega_{turb} \cdot R}{V_{vent}} \quad (4)$$

2.2.3 Mechanical Torque of the Wind Turbine

The mechanical torque calculated by:

$$C_{aer} = \frac{P_{aer}}{\Omega_{turb}} = \frac{1}{2} \cdot \rho \cdot \pi \cdot R^2 \cdot C_p(\lambda, \beta) \cdot V_{wind}^3 \cdot \frac{1}{\Omega_{turb}} \quad (5)$$

2.3 Modeling of the Doubly Fed Induction Generator

The doubly Fed Induction Generator (DFIG) is expressed in the (d-q) reference frame rotating at the speed of the stator field (Chatelain, 1990; Caron & Hautier, 1995; Hofmann & Okafor, 2001; Idjarene et al., 2008; Abad et al., 2011; Karad & Thakur, 2021):

2.3.1 Electrical equations of the stator voltages

$$\begin{cases} V_{sd} = R_s i_{sd} + \frac{d\varphi_{sd}}{dt} - \frac{d\theta_s}{dt} \varphi_{sq} \\ V_{sq} = R_s i_{sq} + \frac{d\varphi_{sq}}{dt} + \frac{d\theta_s}{dt} \varphi_{sd} \end{cases} \quad (6)$$

2.3.2 Electrical equations of the rotor voltages

$$\begin{cases} V_{rd} = R_r i_{rd} + \frac{d\varphi_{rd}}{dt} - \frac{d\theta_r}{dt} \varphi_{rq} \\ V_{rq} = R_r i_{rq} + \frac{d\varphi_{rq}}{dt} + \frac{d\theta_r}{dt} \varphi_{rd} \end{cases} \quad (7)$$

2.3.3 Magnetic equations of stator fluxes

$$\begin{cases} \varphi_{sd} = L_s i_{sd} + M_{sr} i_{rd} \\ \varphi_{sq} = L_s i_{sq} + M_{sr} i_{rq} \end{cases} \quad (8)$$

2.3.4 Magnetic equations of rotor fluxes

$$\begin{cases} \varphi_{rd} = L_r i_{rd} + M_{sr} i_{sd} \\ \varphi_{rq} = L_r i_{rq} + M_{sr} i_{sq} \end{cases} \quad (9)$$

2.3.5 Electromagnetic torque equation

By using Park transformation:

$$V_{rq} = [V_{sA,B,C}]^T \cdot [I_{sA,B,C}] + [V_{rA,B,C}]^T \cdot [I_{rA,B,C}] = [V_{sd,q}]^T \cdot [I_{sd,q}] + [V_{rd,q}]^T \cdot [I_{rd,q}] \quad (10)$$

$$P_e = [V_{sA,B,C}]^T \cdot [I_{sA,B,C}] + [V_{rA,B,C}]^T \cdot [I_{rA,B,C}] = [V_{sd,q}]^T \cdot [I_{sd,q}] + [V_{rd,q}]^T \cdot [I_{rd,q}] \quad (11)$$

Taking into account the magnetic equations (11) and (12), the system of electrical equations becomes:

$$\begin{cases} v_{sd} = \left(R_s + L_s \frac{d}{dt}\right) \cdot i_{sd} + M_{sr} \frac{di_{rd}}{dt} - L_s \omega_s i_{sq} - M_{sr} \omega_s i_{rq} \\ v_{sq} = \left(R_s + L_s \frac{d}{dt}\right) \cdot i_{sq} + M_{sr} \frac{di_{rq}}{dt} - L_s \omega_s i_{sd} - M_{sr} \omega_s i_{rd} \\ v_{rd} = \left(R_r + L_r \frac{d}{dt}\right) \cdot i_{rd} + M_{sr} \frac{di_{sd}}{dt} - L_r \omega_r i_{rq} + M_{sr} \omega_r i_{sq} \\ v_{rq} = \left(R_r + L_r \frac{d}{dt}\right) \cdot i_{rq} + M_{sr} \frac{di_{sq}}{dt} - L_r \omega_r i_{rd} + M_{sr} \omega_r i_{sd} \end{cases} \quad (12)$$

2.4 Control System of Rotor Side Converter and Grid Side Converter

The Power Maximization Block oversees the execution of Maximum Power Point Tracking (MPPT) algorithms. MPPT guarantees optimal operation of the wind turbine by continually adjusting the generator's operating point to align with fluctuating wind conditions.

2.4.1 Rotor Current Control Loops

Nonetheless, as depicted in Figure 2, utilizing equal proportional-integral (PI) regulators for both current control loops leads to certain outcomes (Tamvada & Babu, 2022).

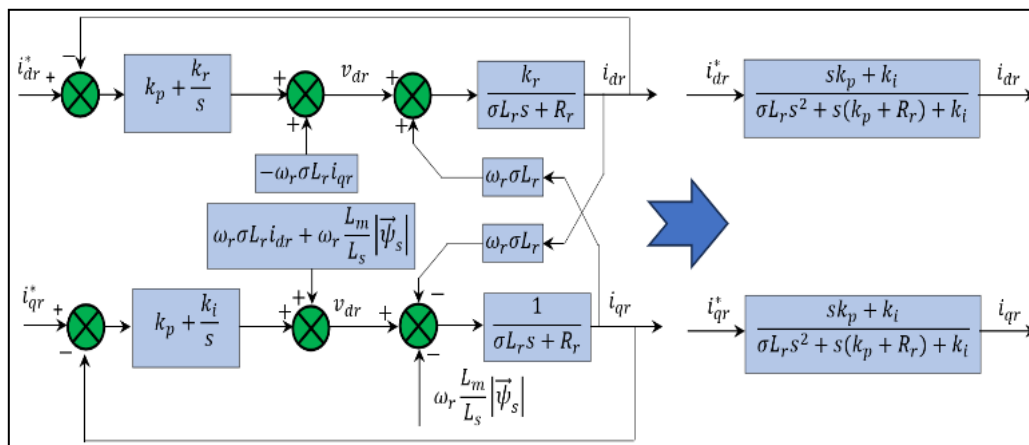


Fig 2. System of closed loop current control with PI regulator

2.5 The RSC control block

This block pertains to the control mechanism governing the Rotor-Side Converter (RSC). The RSC is tasked with managing power transmission between the generator's rotor and the DC link. It oversees the regulation of rotor currents, facilitating efficient power extraction from the wind.

2.6 The GSC control block

This block denotes the control system designed for the Grid-Side Converter (GSC). The GSC is responsible for overseeing power transmission between the DC link and the grid. It ensures synchronization of the generator's output with the grid's voltage and frequency, and it regulates the active and reactive power injected into the grid.

2.7 Crowbar Protection

Voltage sags, resulting from incidents or faults within the electrical network, are the focus of this study. Specifically, it addresses symmetrical voltage sags. According to grid regulations, wind turbines are required to possess Low Voltage Ride Through (LVRT) capability, ensuring they remain connected to the grid during significant voltage sags. To safeguard the system against potential overcurrents and overvoltages during such events, a crowbar protection mechanism is employed. This protection is linked to the rotor and can be activated and deactivated without disconnecting the Doubly Fed Induction Generator (DFIG) from the grid. Figure 2 illustrates the connection of the crowbar protection to the rotor for the protection of the Rotor-Side Converter (RSC).

3. SIMULATION RESULTS

The efficiency of the crowbar protection in safeguarding the DFIG is assessed by evaluating the wind turbine's performance in both normal and abnormal scenarios. Following the symmetrical voltage sags at 3 seconds, where the voltage declines to 90% of its nominal value, disruptions may occur if the rotor current (I_r) surpasses the current threshold ($I_{r\text{limit}}$) or if the DC bus voltage (V_{bus}) exceeds the voltage threshold (V_{buslimit}). During this period, the crowbar protection is automatically triggered by monitoring these two parameters (I_r , V_{bus}). Typically, the current surpasses its threshold first. Upon detecting the voltage sag, the crowbar protection is activated in under 100 milliseconds. The ensuing diagram illustrates the sequence of events during this process. Figures 3 to 5 portray the fluctuations in various system variables, accompanied by an effort to elucidate the observed alterations:

3.1 Variation of current CROWBAR

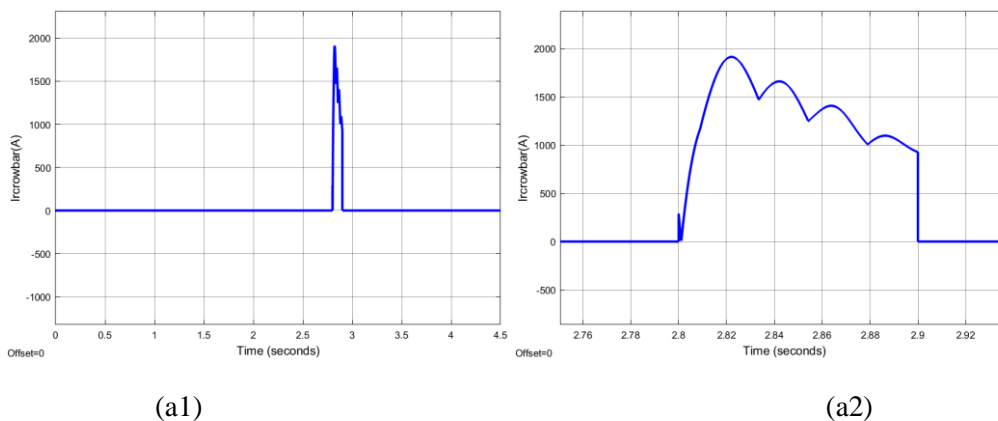
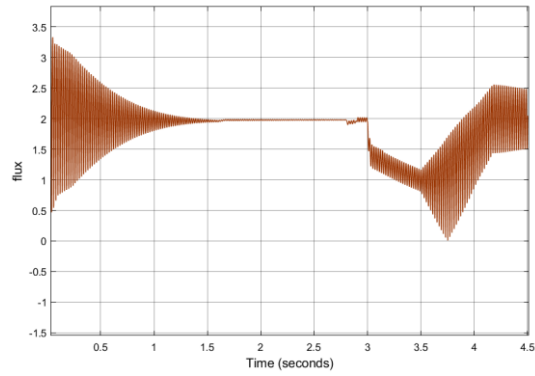


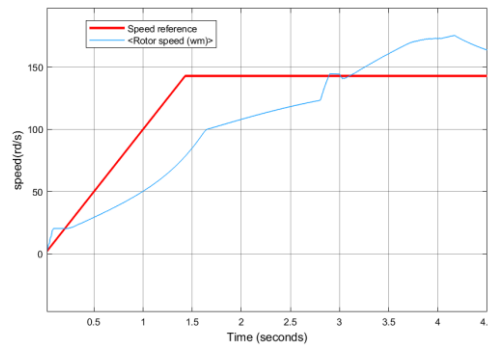
Fig 3. a1) current CROWBAR. a2) Zoom b1) F_s , Stator flux



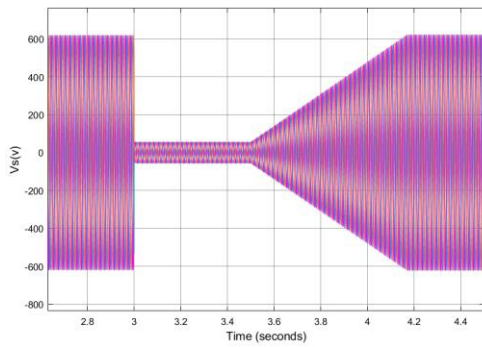
(b1)

Fig 3. a1) current CROWBAR. a2) Zoom b1) Fs, Stator flux (continued)

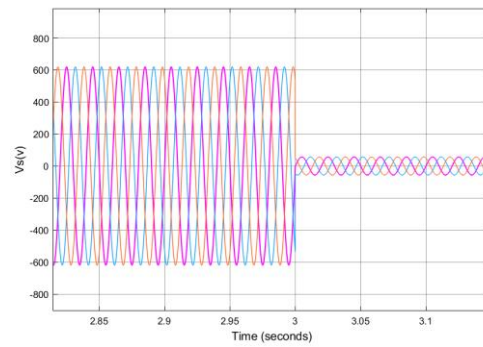
3.2 Variation of rotor side converter variables RSC



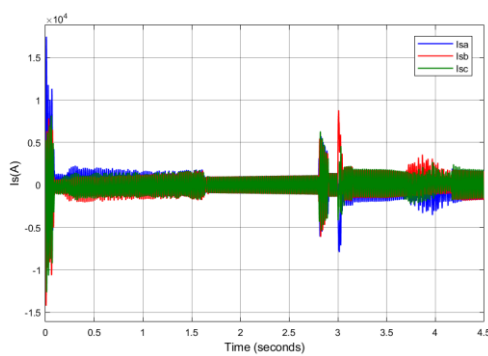
(a)



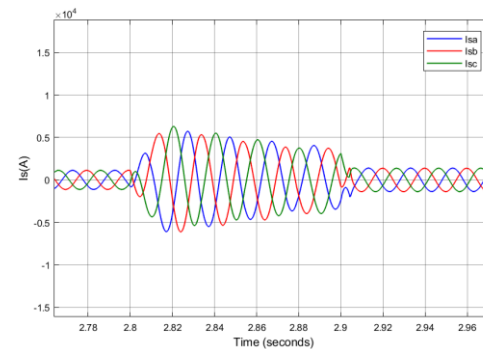
(b1)



(b2)



(c1)



(c2)

Fig 4. Presentation of different rotor side converter variables RSC

a) Rotor speed, b1) Vs, Stator voltage, b2) Zoom c1) Is, Stator current, c2) Zoom

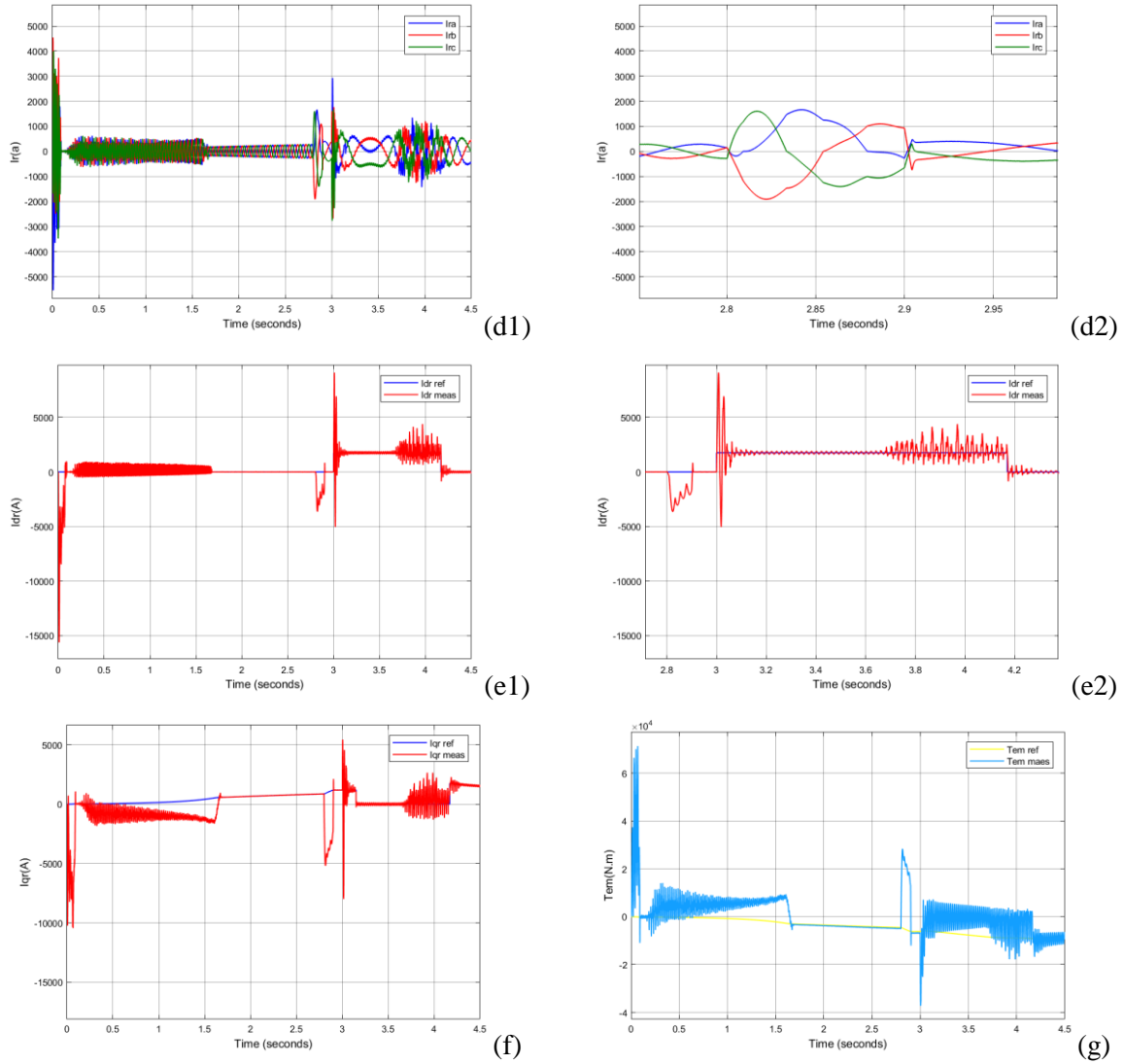


Fig 4. Presentation of different rotor side converter variables RSC (*Continued*)
 d1) I_r , Rotor current, d2) Zoom e1) I_{dr} , Direct rotor current, e2) Zoom f) I_{qr} , quadratic rotor current
 g) T_{em} , Torque

3.3 Variation of grid side converter variables GSC

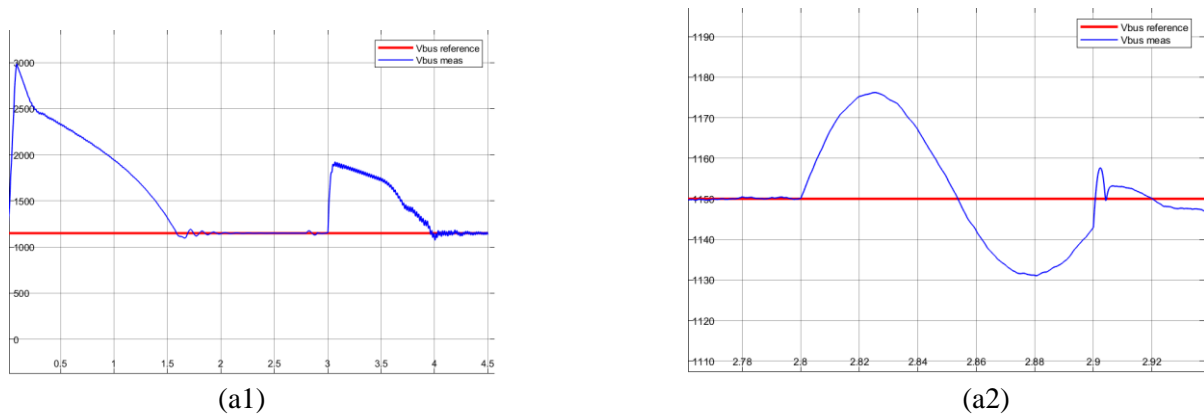


Fig 5. Presentation of different grid side converter variables GSC a1) V_{bus} , Bus voltage. a2) Zoom

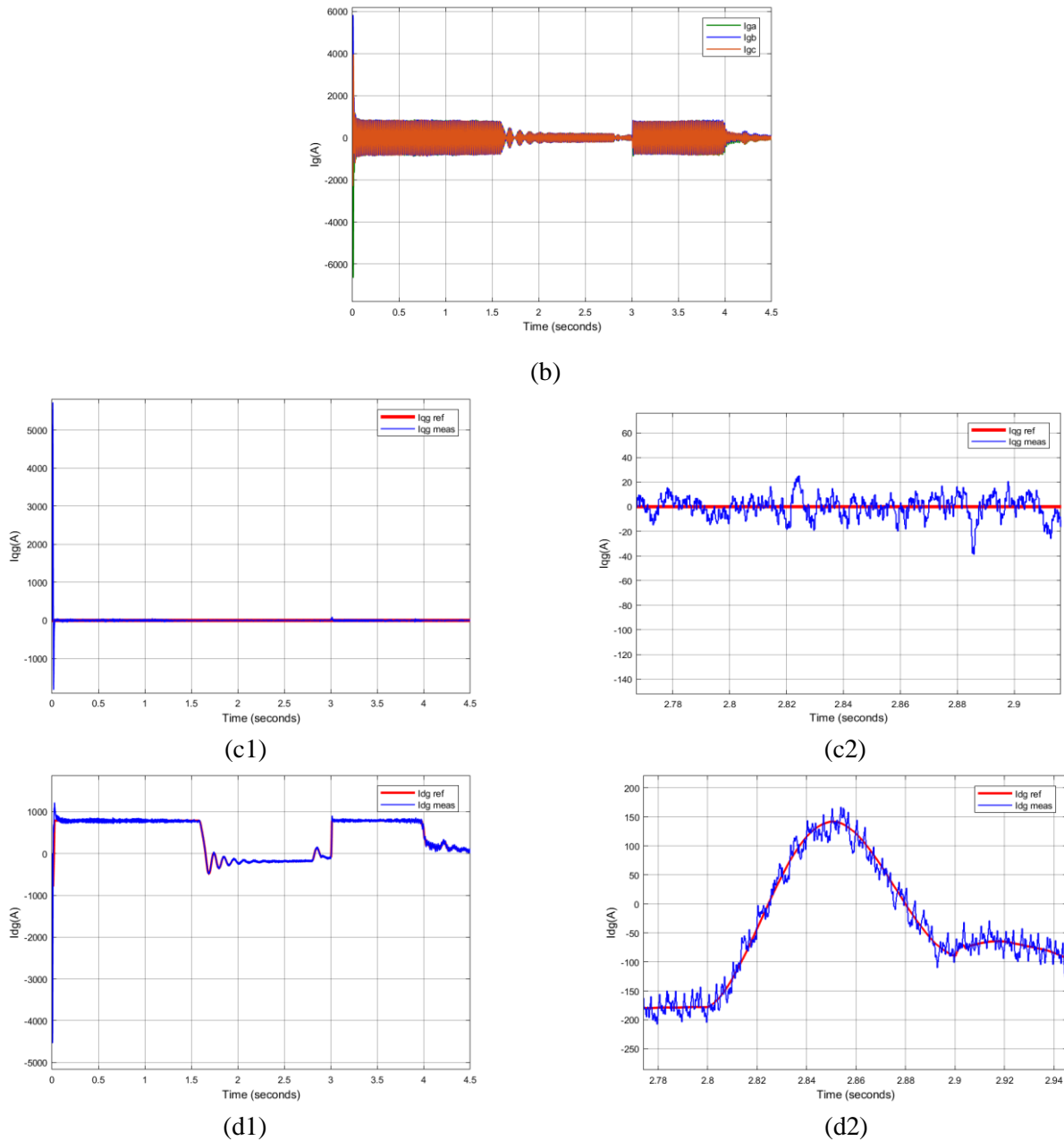


Fig 5. Presentation of different grid side converter variables GSC (Continued)

b) I_g , Grid current, c1) I_{qg} , Quadratic grid current, c2) Zoom d1) I_{dg} , Direct grid current, d2) Zoom

Our aim is to provide precise explanations for the fluctuations observed in these variables. In Figures 3 (crowbar), it is evident that during this period, the peak current flows through the crowbar resistance, resulting in a rapid variation in crowbar current between 2.8 and 2.9 seconds. Additionally, the figures illustrate oscillations in the flow (flux), with its value decreasing swiftly during crowbar operation before gradually returning to its baseline over time.

In figures 4.b and 4.c, concerning the stator voltages (Vs) and stator currents (is), it is observed that at 2.8 seconds, the stator voltages (Vs) drop to 90% of their nominal value, leaving only 10% of the voltage remaining at the grid. Furthermore, there is an impact on the stator currents (is), peaking at 2.8 seconds before reverting back to their sinusoidal waveform.

In Figure 4.d, which represents the rotor current (I_r), it is evident that during voltage dips, there is a temporary decrease in the grid voltage. This situation can lead to a reduction in the magnetic flux within

the machine, necessitating a sudden surge in rotor current to uphold power equilibrium and offset the voltage decline.

At the onset of the voltage dip, precisely at 2.8 seconds as depicted in Figure 4.a (speed), there is a noticeable decline in rotor speed followed by a subsequent rise. This phenomenon occurs due to the decrease in grid voltage, which in turn reduces the stator voltage of the Doubly Fed Induction Generator (DFIG). Despite the constant mechanical power supplied by the wind, the rotor speed decreases initially to maintain power balance. This loss of speed control causes the speed to drop until it falls below the synchronous speed ($N_r > N_s$). At this juncture, the rotor currents remain relatively constant, indicating operation in a hypersynchronous state.

In Figure 4.g (torque), it is evident that the peak of electromagnetic torque coincides with the peak of crowbar current, indicating an unavoidable association between the two. Subsequently, the torque oscillates around zero before eventually returning to its normal setpoint. This fluctuation in torque can be attributed to the decrease in grid voltage, causing a reduction in magnetic flux and consequently leading to a decrease in the electromagnetic torque generated by the generator. As a consequence, the torque oscillates around zero, demonstrating a relatively low disturbance rejection time.

Upon resolution of the voltage dip and restoration of grid voltage to its normal level, the control strategy governing the Doubly Fed Induction Generator (DFIG) readjusts the parameters of the Rotor-Side Converter (RSC) to return the electromagnetic torque to its standard operating level. This action ensures the system maintains stable operation.

Regarding the performance of the rotor side converter, illustrated in Figures 4.f (i_{qr}), it can be observed that at the onset of voltage dips, the current i_q is deliberately set to zero, resulting in zero torque output. Nonetheless, oscillations occur due to the voltage dips. This phenomenon is attributed to the necessity of torque by the maximum power point tracking algorithm to regulate the speed.

During instances of symmetrical voltage dips, as mandated by the grid codes, showcased in Figures 4.e (i_{dr}), a significant value of i_d rotor current is deliberately applied to generate reactive power through the stator by introducing this current component.

Figures 5.a (VBUS) depict the fluctuation of V_{buc} , which exhibits oscillations around its reference voltage set at 1200 V. Maintaining stability in the voltage across this capacitor is imperative for the proper functioning of the system. This is achieved through the Capacitor Control Regulator (GSC).

In Figures 5.c and 5.d, it is evident that the variations in grid currents and voltages (i_{qgrid} , i_{dgrid}) during disturbances follow similar patterns. During a voltage dip, the grid currents experience oscillations around their nominal values. Once the voltage dip subsides, the system's control strategies restore the grid currents and voltages to their nominal values, thereby ensuring the stable operation of the system.

4. CONCLUSION

The results obtained in this study demonstrate the impact of symmetrical voltage dips on the performance of doubly fed induction generator (DFIG) wind turbines. Analyzed figures reveal variations in electrical and mechanical quantities, as well as the influence of protection and regulation strategies on system stability. During symmetrical voltage dips, stator voltages decrease significantly, leading to transient variations in stator currents. Rotor currents increase abruptly to compensate for the voltage drop and maintain power balance. These variations can impact system stability, especially rotor speed and magnetic flux. Protection strategies, such as using crowbar resistances, play a crucial role in maintaining the wind turbine's connection to the grid during symmetrical voltage sags. This ensures continuous energy production and limits transient variations in electrical quantities. Regulation

strategies also contribute to mitigating the effects of disturbances. They help minimize rotor speed variations and maintain stable system operation. Regulation of both rotor-side and grid-side converters is crucial to ensuring a rapid and effective response to symmetrical voltage dips and maintaining system stability. The results underscore the importance of optimizing control parameters to ensure optimal DFIG wind turbine performance in the presence of electrical disturbances. Recommendations can be made to improve protection and regulation strategies, ensuring system stability and equipment protection. In conclusion, this study highlights the importance of understanding and managing the effects of symmetrical voltage dips on DFIG wind turbines. The findings can be used by wind farm designers and electric grid operators to enhance the reliability and performance of DFIG wind turbine systems, contributing to the effective integration of renewable energies into the electrical grid.

REFERENCES

- Abad, G., et al. (2011). *Doubly Fed Induction Generators Control for Wind Energy*. Hoes Lane Piscataway, 633 p.
- Canudas de Wit, C. (2000). *Commande des moteurs asynchrone, Modélisation contrôle vectoriel et DTC* (Vol. 1). Lavoisier, Paris.
- Caron, J.P., & Hautier, J.P. (1995). *Electrotechnique: Modélisation et commande de la machine asynchrone*. Presses Universitaires de Strasbourg.
- Chatelain, J. (1990). *Machines Electriques*.
- Csanyi, E. (2013, June 7). Impacts of voltage dips on power quality problems. *Electrical Engineering Portal*. <http://electrical-engineering-portal.com/impacts-of-voltage-dips-on-power-quality-problems>
- Hofmann, W., & Okafor, F. (2001). Optimal control of doubly-fed full-controlled induction wind generator with high efficiency. *IECON'01: 27th Annual Conference of the IEEE Industrial Electronics Society*, 1213–1218. <https://doi.org/10.1109/IECON.2001.975955>
- Hughes, A. (2005). *Electric motors and drives: Fundamentals, types, and applications*. Energy Conversion Management, 101, 681–688.
- Idjdarene, K., Tounzi, A., Rekioua, D., & Rekioua, T. (2008). Vector control of autonomous induction generator taking saturation effect into account. *Energy Conversion and Management*.
- Karad, S., & Thakur, R. (2021). Recent trends of control strategies for doubly fed induction generator based wind turbine systems: A comparative review. *Arch Computat Methods Eng*, 28, 15–29. <https://doi.org/10.1007/s11831-019-09367-3>
- Rabelo, B., Hofmann, W., Silva, J. L., Oliveira, R. G., & Silva, S. R. (2008). Reactive power control in doubly-fed induction generators for wind turbines. *IEEE Power Electronics Specialists Conference*, 106-112. <https://doi.org/10.1109/PESC.2008.4591908>
- Seyoum, D., Grantham, C., & Rahman, M. F. (2003). The dynamic characteristics of an isolated self-excited induction generator driven by a wind turbine. *IEEE Transactions on Industry Applications*.
- Tamvada, K., & Babu, R. (2022). Control of doubly fed induction generator for power quality improvement: An overview. *International Journal of System Assurance Engineering and Management*, 13, 2809–2832. <https://doi.org/10.1007/s13198-022-01754-7>